Numerical Analysis of Arbitrarily Shaped Bodies Modeled by Surface Patches

JOHNSON J. H. WANG, SENIOR MEMBER, IEEE, AND CHARLES J. DRANE, SENIOR MEMBER, IEEE

Abstract—**Numerical modeling techniques for arbitrarily shaped conducting bodies using triangular surface patches are presented. Computer codes based on the magnetic field integral equations, the electric field integral equations, and the reaction integral equations were developed and tested with various degrees of success.**

I. Introduction

MANY FREE-SPACE scattering and radiation problems can be readily analyzed by the wire-grid modeling technique [1]–[3] for which a number of well-tested thin-wire moment-method codes have been developed. However, these wire-grid models have certain limitations [4], [5] and are dependent on the user's judgement on such issues as appropriate choice of wire diameter in the computation. As a result, there is an increasing level of interest in modeling arbitrarily shaped bodies by surface patches [6]–[15].

The analysis of surfaces is considerably more complex than that of thin-wire structures. Consequently, computer codes based on surface models tend to be more time consuming than wire-grid codes. In this paper, three surface-patch modeling techniques and their numerical results are presented. The first method is a modified version of an earlier Magnetic Field Integral Equation (MFIE) algorithm [11]. The second method utilizes the reaction integral equation but was not fully tested because it requires a prohibitively large computer run time. The third method is an Electric Field Integral Equation (EFIE) algorithm for handling thin-shell scatterers which cannot be dealt with by the MFIE code. Numerical testing and evaluation of a variety of geometries were carried out on the CDC Cyber 74/6400 computer at Georgia Tech and the CDC 6600 computer at Hanscom Field.

In all three computer codes, planar triangular patches are used to model the surfaces. For the MFIE and EFIE codes, pulse functions are chosen as the basis functions, and the impulse function as the test function. The solution is by the well-known method of moments [16], which converts the vectorial integral equations into linear scalar matrix equations solvable on a digital computer.

Manuscript received December 7, 1981; revised March 16, 1982. This work was supported in part by Deputy for Electronic Technology (RADC/ET), Air Force Systems Command, under Contract F19628-78-C-0224.

J. J. H. Wang is with the Engineering Experiment Station, Georgia Institute of Technology, Atlanta, GA 30332.

C. J. Drane is with the Electromagnetic Sciences Division, Home Air Development Center, Hanscom Air Force Base, Bedford, MA 01731.

II. The MFIE Approach

The basic MFIE code, which is based on an expansion of subsectional pulse functions on planar triangular surface patches and point-matching (testing by impulse functions), has been reported in [11]. A major advantage, and simultaneously a limitation as well, of this approach is that the integral in the self-patch matrix element is neglected in the computation. The integral takes the following form:

$$I_n^m = f_{\Delta S_n} \nabla' \phi(\boldsymbol{r}_m, \boldsymbol{r}')\, ds' \tag{1}$$

where

ϕ $= [\exp(-jk|\boldsymbol{r}_m - \boldsymbol{r}'|)]/|\boldsymbol{r}_m - \boldsymbol{r}'|$,
$\boldsymbol{r}_m, \boldsymbol{r}'$ vectors from the origin to the field and source points,
f principal value integral,
∇' gradient operator with respect to the primed coordinates, and
ΔS_n the nth surface patch.

It can be shown that for an equilateral triangular patch small in comparison with the operating wavelength

$$I_n^n \cong 0. \tag{2}$$

Thus the neglect of this integral whose integrand is singular is well justified. Although the proof is based on the assumption of an equilateral triangle, I_n^n departs only gradually and smoothly from (2) for triangles of unequal sides. The proof of (2) is straightforward but quite lengthy [17].

The improvements of the computer algorithm include the reduction of computational time and storage space for symmetrical scatterers, for which the reduction of matrix size to either one-half or one-fourth of the original size depends on whether one-plane or two-plane symmetry exists. An effort to achieve a symmetrical matrix as had been accomplished in some thin-wire programs [2] was unsuccessful. In fact, our observation indicates that matrix symmetry is directly related to the self-conjugate property of the linear operator in the integral equation. As long as the operator in MFIE is not self-conjugate, one will be unable to achieve matrix symmetry. On the other hand, there is a one-to-one correspondence between a self-conjugate operator and a symmetrical matrix in any linear space defined in any orthonormal basis [18].

Numerical computations have been performed previously for smooth conducting bodies such as the sphere and the prolate spheroid [11], [19]. It is of interest to consider

0018-9480/82/0800-1167$00.75 ©1982 IEEE

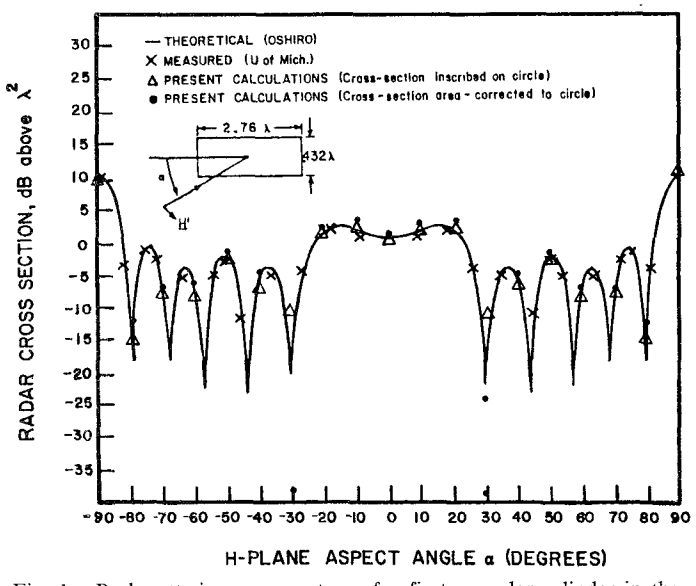

Fig. 1 Backscattering cross section of a finite circular cylinder in the H-plane.

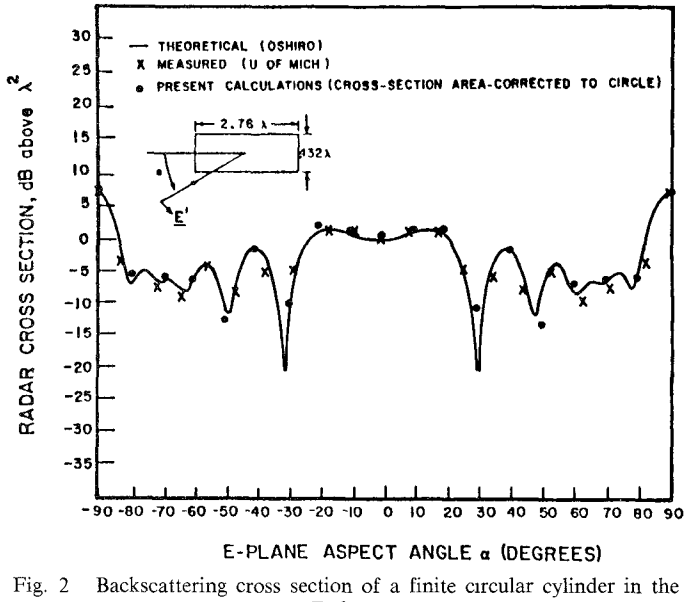

Fig. 2 Backscattering cross section of a finite circular cylinder in the E-plane.

other geometries with edges such as the finite-length circular and rectangular cylinders. The results of the computation for such geometries were then compared with existing data in the literature. While excellent agreement was observed between known data and the present computation, there was an apparent discrepancy with respect to polarization in some of the cases being considered. Namely, our TE calculation may agree with known data of TM case, and our TM case may agree with some other known TE data in the literature. In fact, our results agree with some sources and disagree with some other sources as far as the incident polarization is concerned. At this point, we tentatively assume that the discrepancy is due to confusion in data presentation with respect to denoting the polarization. A further examination of the literature may resolve this apparent notational problem.

With the foregoing discussion in mind, we present the numerical results, which are in good agreement with existing data in the literature if we ignore these discrepancies in polarization. In the simulation of a finite circular cylinder with surface patches, two methods were used in the handling of the effective diameter of the circular cylinder in the simulation. Either the vertices of the triangle are on the cylinder surface (cross section inscribed on circle) or the vertices are on an enlarged cylinder with the same cross-sectional area (cross-sectional area corrected on circle). The

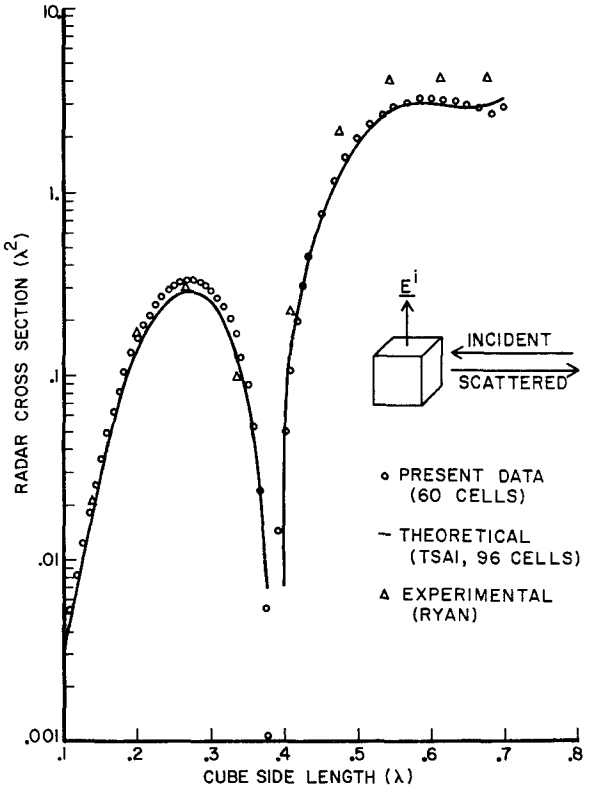

Fig. 3. Comparison of the computed radar cross section of a conducting box with other known data.

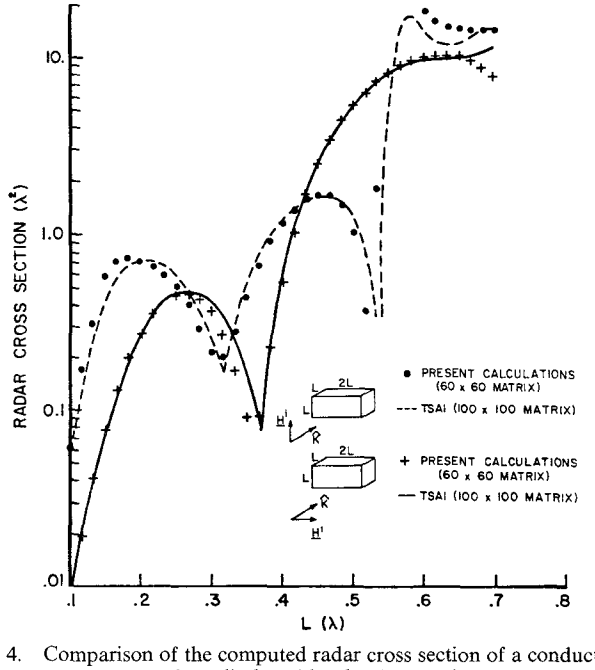

Fig. 4. Comparison of the computed radar cross section of a conducting rectangular cylinder with other known data.

computed results are compared in Figs. 1 and 2 with known data in the literature [4], [6], [9]. Comparison was also made with the measured data of Carswell [20] and Mack [21] with satisfactory agreement. The area-corrected computation using an effective diameter larger than the cylinder diameter appears to be in closer agreement with known data.

Figs. 3 and 4 show the computed results for a rectangular cylinder, of which the cube is a special case, in comparison with known data [7]. Apparently, wedges of 90° pose no difficulty in the MFIE computation.

The computational speed and central memory requirement are dependent on the number of patches used in the simulation. For a 96-patch spheroid, which nearly occupies the full central memory of the CDC Cyber 74 computer at Georgia Tech, one run at a single frequency and one incidence angle takes about 150 CPU's. For symmetrical scatterers, the execution time and central memory requirements are reduced by 75 percent. When there is two-plane symmetry, this reduction is 94 percent. Thus, for the sphere, in which two-plane symmetry exists, the execution time is 9 s and the central memory size will be one sixteenth of that required by one with no symmetry.

III. The Reaction Integral Equation Approach

The reaction integral equation has been applied to the special case of a rectangular plate and a dihedral corner reflector [8]. The possibility of using this approach for arbitrarily shaped scatterers is examined here. The major difficulty in this approach lies in the difficulties in the integration to obtain the matrix elements given by

$$Z_{mn}^{ij} = -\int_{\Delta S_m} \boldsymbol{J}_m^i \cdot \boldsymbol{E}_n^j \, ds \tag{3}$$

where

$\boldsymbol{J}_m^i$ basis function of ith polarization in the mth patch
$\boldsymbol{E}_n^j$ electric field due to the basis function of jth polarization in the nth patch.

Strictly speaking, (3) involves two double integrations, as $\boldsymbol{E}_n^j$ must also be evaluated by an integration process. Presently, there appears to be no closed-form expression for the field of a triangular current patch. Even in the case of a finite line source, the sinusoidally excited thin dipole is probably the only one with a simple closed-form expression for the near-zone field [2]. In order to compute $\boldsymbol{E}_n^j$ in (3), two integration methods were tried. The first method employs numerical integration techniques, and the second method is based on the approximation of the surface current with several line current elements.

In the numerical integration technique, a definite integral is expanded into a finite series which can be computed numerically [22]. Specifically, the integration of a function over a triangular area can be carried out with a 64-point formula. 64 points in the triangle are preselected according to a simple arithmetic formula, and the values of the integrand at these points are then computed. The value of the integral is then obtained by summing up the product of these 64 sampled integrands and a predetermined weighting function of simple arithmetic form.

S_z/λ	S_y/λ	Wang Richmond Gilreath	Present Calculation
0	0.25	39.07 - j22.49	38.92 + j70.31
0	0.50	- 8.659 - j26.75	- 8.589 - j26.56
0.25	0.25	29.54 - j 9.070	29.42 - j36.79
0.50	0.50	- 9.568 - j 6.65	- 9.484 - j 6.574

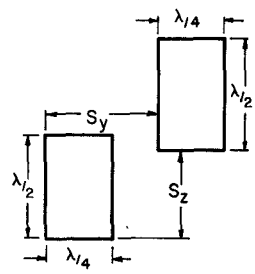

Fig. 5. Comparison of computed mutual impedances between two rectangular dipoles.

The accuracy of the numerical integration depends on how rapidly and frequently the value of the integrand varies in the area of integration. The 64-point algorithm was checked with several known functions, and the accuracy of this algorithm was quite impressive. For example, a comparison between the exact values and the results of numerical integration for the integral

$$\int_0^1 \int_0^{1-x} \sin \omega x \, dy \, dx \tag{4}$$

shows that even when $\omega = 50$ the 64-point algorithm is accurate within 1 percent.

Although this integration algorithm is highly accurate, it is inefficient. Consequently, considerable restraint must be exercised in applying this technique to the evaluation of matrix elements in (3). Since we were unable to obtain a closed form analytical expression for $\boldsymbol{E}_n^j$ in (3), we chose to approximate the patch current with orthogonal current filaments. Obviously, the higher the number of filaments included in the process, the more accurate will be the approximation.

The expressions for the electric field radiated from a line current having a sinusoidal distribution were well documented by Schelkunoff and Friis [23]. Because of the symmetry of a straight line current, the radiated field is constant around the axis of the line current. The radiated field therefore consists of two components, one parallel to the current and one perpendicular to the current. There is no ϕ component if a cylindrical coordinate is assigned with the current being along the z-axis. A check of the formulas for E_ρ and E_z showed that E_ρ was an exact expression. However, the expression for E_z was not an exact expression as implied in [23].

Fig. 5 shows a comparison between the present calculation and the calculated data in [8] for the mutual impedance between two rectangular dipoles. The present calculation employed a three-filament approximation for triangular surface patches. Each rectangular patch was divided diagonally into two triangular patches. The agreement is

good as long as the dipoles are spaced one quarter wavelength away. For closely spaced dipoles, more current filaments are needed in the approximation.

This combined analytical-numerical method made it possible to reduce drastically the computational time required for the matrix element to about 1/20 of the time needed for the previous numerical integration. However, the requirement for computational time was still prohibitively high. Presently, there appears to be no readily available technique to reduce the CPU time to a more desirable level.

IV. The EFIE Approach

The electric field integral equation takes the following form [4]:

$$\hat{n}\times \boldsymbol{E}^{\text{inc}}(\boldsymbol{r}) = \frac{1}{4\pi j\omega\varepsilon}\hat{n}\times \int_s \{-\omega^2\varepsilon\mu \boldsymbol{J}_s(\boldsymbol{r}')\phi(\boldsymbol{r},\boldsymbol{r}') + [\nabla'_s\cdot \boldsymbol{J}_s(\boldsymbol{r}')]\nabla'\phi(\boldsymbol{r},\boldsymbol{r}')\}\, ds' \quad (5)$$

where

$\boldsymbol{E}^{\text{inc}}(\boldsymbol{r})$ incident electric field

$\nabla'_s = \hat{t}_1\frac{\partial}{\partial t_1} + \hat{t}_2\frac{\partial}{\partial t_2}$, and

$\hat{t}_1, \hat{t}_2$ two orthogonal unit vectors on the surface S.

We denote the right-hand side of (5) with an operator form $\mathfrak{L}(\boldsymbol{J}_s(\boldsymbol{r}'))$ and rewrite it as

$$\mathfrak{L}(\boldsymbol{J}_s(\boldsymbol{r}')) = \hat{n}\times \boldsymbol{E}^{\text{inc}}(\boldsymbol{r}). \quad (6)$$

Furthermore, we let

$$\mathfrak{L} = \mathfrak{L}_1 + \mathfrak{L}_2 \quad (7)$$

where $\mathfrak{L}_1$ and $\mathfrak{L}_2$ refer to the terms involving $\boldsymbol{J}_s$ and $\nabla'_s\cdot\boldsymbol{J}_s$ in (5), respectively.

In (5), the unknown current $\boldsymbol{J}_s$ appears in two forms: $\boldsymbol{J}_s$ and $\nabla'_s\cdot\boldsymbol{J}_s$. If $\boldsymbol{J}_s$ is chosen to be a pulse function, then $\nabla'_s\cdot\boldsymbol{J}_s$ will be singular at the edge of the triangular cells. A similar problem exists in the analyses of thin-wire scatterers and bodies of revolution. For example, Harrington and Mautz [16], [24] solved the single straight-wire problem with pulses as basis functions and delta functions for testing. In comparison with a method using triangular functions for testing, there was no significant difference in the results observed as long as the segments are less than $\lambda/10$ in length. In the analyses of the scattering from bodies of revolution, Mautz and Harrington [25] preferred the triangular functions to a pulse function as the basis. However, in the process of evaluating the matrix elements, the triangular function is approximated by four pulse functions in one integration and four impulse functions in another integration. The derivative of the basis function is approximated by four pulse and impulse functions correspondingly. Thus the handling of the derivative of the current is not very restrictive in these earlier computations.

Based on the tradeoff between the expected efficiency and accuracy of the computation, the pulse function was first chosen as the basis function for the expansion of the unknown current. For this basis expansion, the delta function is appropriate and compatible for testing as has been observed in the MFIE algorithm. A major difficulty, as has been discussed, is the handling of the term $\nabla'_s\cdot\boldsymbol{J}_s$ in (5), which can be dealt with in several ways. A series of numerical tests were performed for these various schemes but none of them was found satisfactory. Finally, a basis function was selected and defined as follows. The surface current is expanded as

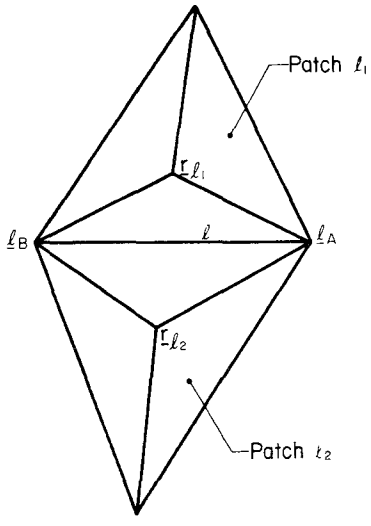

Fig. 6. Subdividing the two adjacent triangular patches, patch l_1 and patch l_2.

$$\boldsymbol{J}_s = \sum_{n=1}^{N} \boldsymbol{J}_n \quad (8)$$

where n is the index of the individual triangular patch and

$$\boldsymbol{J}_n = I_n^1\boldsymbol{J}_n^1(\boldsymbol{r}) + I_n^2\boldsymbol{J}_n^2(\boldsymbol{r}). \quad (9)$$

$\boldsymbol{J}_n^1$ and $\boldsymbol{J}_n^2$ are two vectorial functions which satisfy

$$\boldsymbol{J}_n^j(\boldsymbol{r}_n) = \boldsymbol{U}_n^j, \qquad j=1,2 \quad (10)$$

where $\boldsymbol{r}_n$ is the positional vector of the center of the nth patch, and $\boldsymbol{U}_n^1$ and $\boldsymbol{U}_n^2$ are unit orthogonal vectors.

In order to evaluate $\nabla'_s\cdot\boldsymbol{J}_s$, we divide each triangular patch into three triangles by connecting each vertex with the center of the bisectors as shown in Fig. 6. We then approximate the diagram of current by

$$\begin{aligned}\nabla'_s\cdot\boldsymbol{J}_s &= \nabla'\cdot\boldsymbol{J}_s - \hat{u}_n\cdot\frac{\partial \boldsymbol{J}_s}{\partial n}\\ &\cong \nabla'\cdot\boldsymbol{J}_s\\ &= \sum_{k=1}^{3}\frac{J_{l_2}^k - J_{l_1}^k}{r_{l_2}^k - r_{l_1}^k}\end{aligned} \quad (11)$$

in the two subtriangles on each side of edge l. The edge index l runs from 1 to L. Also in (11)

$$\begin{aligned}J_{l_i}^k &= \boldsymbol{J}_{l_i}\cdot\hat{u}_k\\ r_{l_i}^k &= \boldsymbol{r}_{l_i}\cdot\hat{u}_k\end{aligned} \quad (12)$$

and $\hat{u}_k$ refers to the unit vectors $\hat{x}, \hat{y}, \hat{z}$ for $k=1,2,3$, respectively. Note that the expansion of the term involving $\nabla'_s\cdot\boldsymbol{J}_s$ is in terms of the edge index l while that for the $\boldsymbol{J}_s$ term is by patch number n.

We now test the integral (5) with a weighting function

defined as

$$w_n^i(\boldsymbol{r}) = \delta(\boldsymbol{r}-\boldsymbol{r}_n)\boldsymbol{u}_n^i. \tag{13}$$

A system of linear equations in the following form can be generated by taking the scalar product

$$\{\boldsymbol{W}_m^i, \mathcal{L}_1(\boldsymbol{J}_s)\} + \{\boldsymbol{W}_m^i, \mathcal{L}_2(\boldsymbol{J}_s)\} = \{\boldsymbol{W}_m^i, \hat{n}\times\boldsymbol{E}^{\text{inc}}\},$$
$$\text{for } i=1,2, \qquad m=1,2,\cdots,N \tag{14}$$

where for $m \neq l_1$ or l_2 (l_1 and l_2 being the patch indices on either side of the edge l)

$$\{\boldsymbol{W}_m^i, \mathcal{L}_1(\boldsymbol{J}_s)\} = \frac{1}{4\pi j\omega\varepsilon}\boldsymbol{u}_m^i\cdot\hat{n}_m \times f_S\{-\omega^2\varepsilon\mu \boldsymbol{J}_s\phi(\boldsymbol{r}_m,\boldsymbol{r}')\,ds'$$
$$\cong \frac{-\omega\mu}{4\pi j}\boldsymbol{u}_m^i\cdot\hat{n}_m \times \sum_{l=1}^{L}\frac{1}{2}(\boldsymbol{J}_{l_1}+\boldsymbol{J}_{l_2})(\Delta S_{l_1}+\Delta S_{l_2})$$
$$\cdot\frac{1}{3}\phi(\boldsymbol{r}_m,\boldsymbol{r}_{lc}). \tag{15}$$

ΔS_{l_k} in (15) denotes the area of patch l_k, and $\boldsymbol{r}_{lc}$ denotes the center of edge l. With this approximation this term becomes equivalent to that for a pulse basis function.

The excitation column matrix in (14) is simply

$$\{\boldsymbol{W}_m^i, \hat{n}\times\boldsymbol{E}^{\text{inc}}\} = \boldsymbol{u}_m^i\cdot\hat{n}_m\times\boldsymbol{E}^{\text{inc}}(\boldsymbol{r}_m). \tag{16}$$

The term involving $\mathcal{L}_2$ is, for $m \neq l_1$ or l_2

$$\{\boldsymbol{W}_m^i, \mathcal{L}_2(\boldsymbol{J}_s)\} = \frac{1}{4\pi j\omega\varepsilon}\boldsymbol{u}_m^i$$
$$\cdot\hat{n}_m\times f_S(\nabla_s'\cdot\boldsymbol{J}_s(\boldsymbol{r}'))\nabla'\phi(\boldsymbol{r}_m,\boldsymbol{r}')\,ds'$$
$$\cong \frac{1}{4\pi j\omega\varepsilon}\boldsymbol{u}_m^i\cdot\hat{n}_m\times\sum_{j=1}^{2}\sum_{l=1}^{L}\frac{1}{2}(t_1^l+t_2^l)C_l$$
$$\left[I_{l_2}^l\sum_{k=1}^{3}\frac{\boldsymbol{u}_{l_2}^j\cdot\hat{u}_k}{r_{l_2}^k-r_{l_1}^k} - I_{l_1}^l\sum_{k=1}^{3}\frac{\boldsymbol{u}_{l_1}^j\cdot\hat{u}_k}{r_{l_2}^k-r_{l_1}^k}\right]\nabla'\phi(\boldsymbol{r}_m,\boldsymbol{r}_{lc}) \tag{17}$$

where t_1^l and t_2^l are distances from $\boldsymbol{r}_{l_1}$ and $\boldsymbol{r}_{l_2}$ to edge l, respectively, C_l is the length of edge l, and $\boldsymbol{r}_{lc}$ is the position vector of the center of edge l.

When $m=l_1$ or l_2, the field point $\boldsymbol{r}_m$ is in the source region, and the integral involving the $\mathcal{L}_1$ and $\mathcal{L}_2$ operators must be carefully handled because of the singular nature of ϕ. Fig. 7 shows how a subtriangle on edge l is approximated by a sector of a circle so that the singular nature of ϕ at $\boldsymbol{r}_m=\boldsymbol{r}_{l_1}$ or $\boldsymbol{r}_{l_2}$ can be accurately calculated. The integral in (5) involving $\mathcal{L}_1$ can be evaluated by using the following relation when $\boldsymbol{r}_m=\boldsymbol{r}_{l_1}$ or $\boldsymbol{r}_{l_2}$:

$$\int_{\Delta S_l}\boldsymbol{J}_s^l\phi(\boldsymbol{r}_m,\boldsymbol{r}')\,ds' \cong \int_0^{R_{l_1}}\int_0^{\psi_{l_1}}\left[\boldsymbol{J}_s^{l_1}+(\boldsymbol{J}_s^{l_2}-\boldsymbol{J}_s^{l_1})\frac{R}{R_l}\right]$$
$$\cdot\frac{e^{-jkR}}{R}R\,dR\,d\phi$$
$$= \boldsymbol{J}_s^{l_1}\psi_{l_1}\left\{\frac{1}{jk}-\frac{e^{-jkR_{l_1}}}{R_{l_1}k^2}+\frac{1}{R_{l_1}k^2}\right\}$$
$$+\boldsymbol{J}_s^{l_2}\frac{\psi_{l_1}}{R_{l_1}}\left\{e^{-jkR_{l_1}}\left(\frac{R_{l_1}}{-jk}+\frac{1}{k^2}\right)-\frac{1}{k^2}\right\} \tag{18}$$

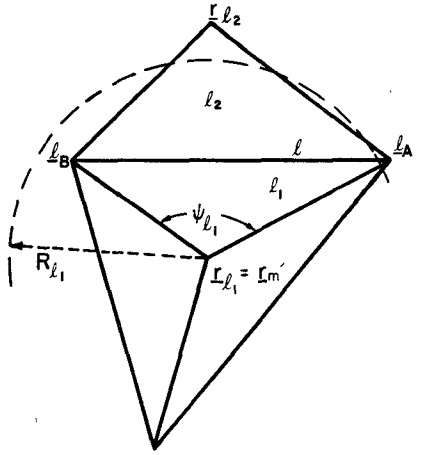

Fig. 7. Approximation of two subtriangles on edge l with a sector of a circle when $\boldsymbol{r}_m=\boldsymbol{r}_{l1}$.

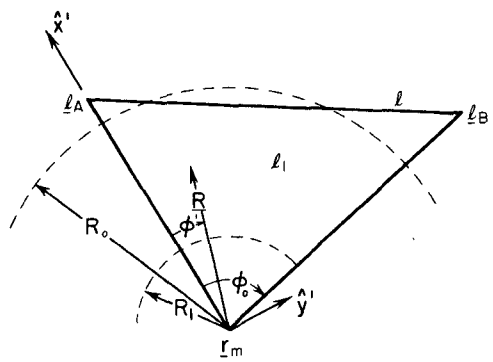

Fig. 8. Approximation of a subtriangle by a sector of a circle when $\boldsymbol{r}_m=\boldsymbol{r}_{l1}$.

where ΔS_l denotes the area of the two subtriangles on either side of edge l and

$$\psi_{l_1} = \left|\cos^{-1}\frac{(\boldsymbol{l}_B-\boldsymbol{r}_m)\cdot(\boldsymbol{l}_A-\boldsymbol{r}_m)}{|\boldsymbol{l}_B-\boldsymbol{r}_m|\,|\boldsymbol{l}_A-\boldsymbol{r}_m|}\right| \tag{19}$$

$$R_{l_1} = \sqrt{\frac{2\Delta S_l}{\psi_{l_1}}}. \tag{20}$$

For the term involving $\mathcal{L}_2$, the scalar product in (17) can be evaluated by the following relation:

$$I = \int_{\Delta S'}\nabla'\phi(\boldsymbol{r}_m,\boldsymbol{r}')\,d\boldsymbol{r}'$$
$$= \int_0^{\phi_0}\int_0^{R_0}\left(-jk-\frac{1}{R}\right)\frac{e^{-jkR}}{R}\hat{R}R\,d\phi'\,dR$$
$$= [\hat{x}'\sin\phi_0+\hat{y}'(1-\cos\phi_0)]\left\{-e^{-jkR_0}+1+\int_{R_1}^{R_0}\frac{e^{-jkR}}{R}dR\right\} \tag{21}$$

where the arguments are illustrated in Fig. 8. Note that the integration from $R=0$ to $R=R_1$, R_1 being a small positive number, can be ignored because

$$\int_0^{2\pi}\int_0^{R_0}\nabla'\phi(\boldsymbol{r}_m,\boldsymbol{r}')R\,dR\,d\phi = 0 \tag{22}$$

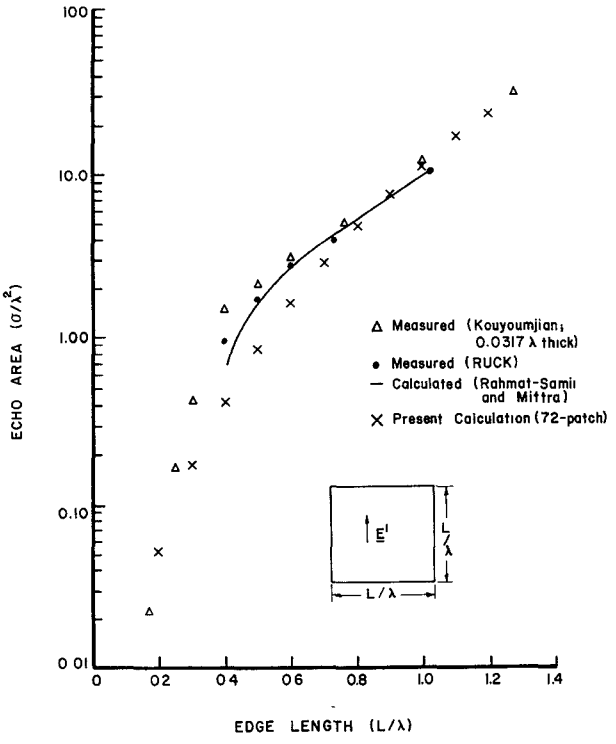

Fig. 9. Convergence test for the EFIE algorithm for the case of a thin-plate scatterer.

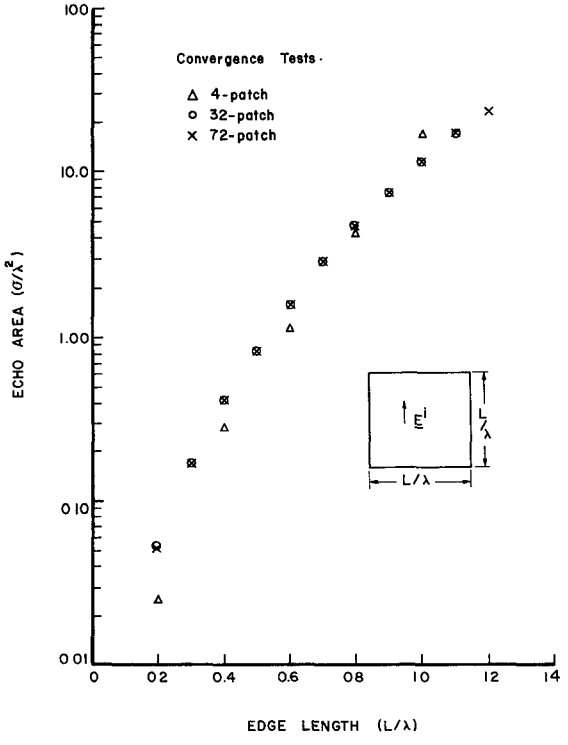

Fig. 10. Comparison of the computed results of the EFIE algorithm and other known data for the case of a thin-plate scatterer.

which follows from (21). Since the integration over the entire surface will cover all the areas, the integration in the neighborhood of $\boldsymbol{r}_m = \boldsymbol{r}_{l1}$ is of the same form as that appearing in (22) which vanishes. The exponential integral in (21) can be evaluated numerically.

If l is a true (physical) edge, the current component

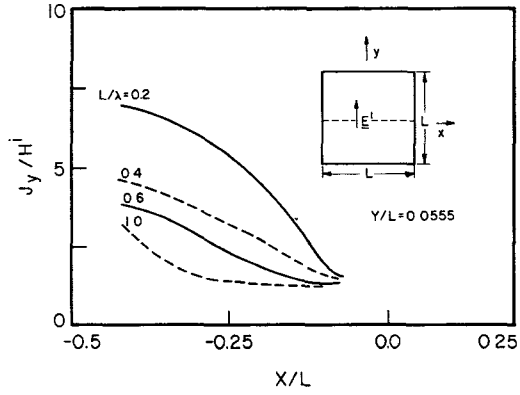

Fig. 11. Current distribution at $Y/L = 0.0555$ on a thin plate illuminated by a normally incident plane wave.

normal to the edge should vanish at the edge. This is handled by either of two methods, both of which have been tested. One is to require that the current on the patch l_1, which had real edge, satisfy

$$\boldsymbol{J}_{l_1} \cdot \hat{n}_{l_1} = 0. \tag{23}$$

In this method, (23) replaces one of the equations in (14) in the solution. Another method, which is used in the computation documented in this report, does not enforce (23) but utilizes the fact that $\boldsymbol{J}_n \cdot \hat{n}_{l_1} = 0$ on the edge in the evaluation of the integrals in the generation of the matrix elements.

Based on the approach described above, an EFIE algorithm was developed and tested numerically for a thin-plate scatterer. Fig. 9 shows the convergence of the computation by using 4, 32, and 72 triangular patches in the simulation. Fig. 10 shows a comparison of the calculated echo area with other known data. Fig. 11 shows the current distribution on a thin plate illuminated by a normally incident plane wave. It was also observed that at the four corners of the plate the calculated current smoothly turns 90°, a phenomenon not reported in the literature.

V. Conclusions

Numerical analyses of arbitrarily-shaped conducting bodies by surface-patch modeling techniques are discussed. Three types of integral equations, the MFIE, EFIE, and reaction integral equations, were used in the numerical analyses. The MFIE appears least time consuming but is unable to handle thin shell structures. The reaction integral equation approach takes a prohibitively large CPU time and appears impractical until either a more efficient integration method, numerical or analytical, is developed or a considerably more powerful computer is available. The EFIE approach, which can handle both smooth closed surfaces and open thin shells and does not involve as much integration as the reaction integral equation approach, therefore deserves greater attention in present-day research.

References

[1] J. H. Richmond, "A wire-grid model for scattering by conducting bodies," *IEEE Trans. Antennas. Propagat.*, vol. AP-14, pp. 782–786, Nov. 1966.

[2] J. H. Richmond, "Radiation and scattering by thin-wire structures

in the complex frequency domain," ElectroSci. Lab., Ohio State Univ., Columbus, OH, Rep. TR2902-10, July 1973.
[3] F. J. Deadrick and E. K. Miller, "A user's manual for the wire antenna modeling program," Lawrence Livermore Lab., Univ. of California, Livermore, CA, Rep. UCID-30084, Dec. 1973.
[4] R. Mittra, Ed., *Numerical and Asymptotic Techniques in Electromagnetics*. New York: Springer-Verlag, 1975.
[5] K. S. H. Lee, L. Marin, and J. P. Castillo, "Limitations of wire-grid modeling of a closed surface," *IEEE Trans. Electromagn. Compat.*, vol. EMC-18, pp. 123-129, Aug. 1976.
[6] F. K. Oshiro, "Source distribution technique for the solution of general electromagnetic scattering problems," in *Proc. First GISAT Symp.*, vol. 1, part 1, Mitre Corp., (Bedford, MA), 1965.
[7] L. L. Tsai, D. G. Dudley, and D. R. Wilton, "Electromagnetic scattering by a three-dimensional conducting rectangular box," *J. Appl. Phys.*, vol. 45, no. 10, pp. 4393-4400, Oct. 1974.
[8] N. N. Wang, J. H. Richmond, and M. C. Gilreath, "Sinusoidal reaction formulation for radiation and scattering from conducting surfaces," *IEEE Trans. Antennas. Propagat.*, vol. AP-23, pp. 376-382, May 1975.
[9] F. K. Oshiro, K. M. Mitzner, and S. S. Locus, "Calculation of radar cross section," Air Force Avionics Lab., Wright-Patterson AFB, OH, Tech. Rep. AFAL-TR-70-21, 1970.
[10] N. C. Albertsen, J. E. Hansen, and N. E. Jensen, "Computation of radiation from wire antennas on conducting bodies," *IEEE Trans. Antennas. Propagat.*, vol. AP-22, pp. 200-206, Mar. 1974.
[11] J. J. H. Wang, "Numerical analysis of three-dimensional arbitrarily-shaped conducting scatterers by trilateral surface cell modeling," *Radio Sci.*, vol. 13, no. 6, pp. 947-952, Nov.-Dec. 1978.
[12] A. W. Glisson and D. R. Wilton, "Simple and efficient numerical methods for problems of electromagnetic radiation and scattering," pp. 593-603, Sept. 1980.
[13] A. W. Glisson and C. M. Butler, "Analysis of a wire antenna in the presence of a body of revolution," *IEEE Trans. Antennas. Propagat.*, vol. AP-28, pp. 604-609, Sept. 1980.
[14] D. R. Wilton, S. S. M. Rao, and A. W. Glisson, "Electromagnetic scattering by surfaces of arbitrary shape," Rome Air Development Center, Griffiss AFB, N.Y., Phase Rep. RADC-TR-79-325, Mar. 1980.
[15] J. R. Mautz and A. T. Adams, "Electromagnetic scattering from a thin rectangular plate," Electromagnetic Compatibility Analysis Center, Annapolis, MD, Rep. ECAC-TN-81-039, July 1981.
[16] R. F. Harrington, *Field Computation by Moment Methods*. New York: Macmillan, 1968.
[17] J. J. H. Wang, "Surface-patch techniques for modeling three-dimensional radiating or scattering objects," Rome Air Development Center, Hanscom Air Force Base, MA., Tech. Rep. RADC-TR-81-41, Apr. 1981.
[18] D. K. Faddeeva and V. N. Faddeeva, *Computational Methods of Linear Algebra*. San Francisco: Freeman, 1963, pp. 85-94.
[19] J. J. H. Wang and C. Papanicolopulos, "Surface-patch modeling of scatterers of arbitrary shapes," in *1979 Int. AP/S Symp. Dig.*, (Seattle, WA) June 1979, pp. 159-162.
[20] A. I. Carswell, "Microwave scattering measurements in the Rayleigh region using a focused-beam syst.," *Can. J. Phys.*, vol. 43, pp. 1962-1977, Nov. 1965.
[21] R. B. Mack, private communication.
[22] A. H. Stroud, *Approximate Calculation of Multiple Integrals*. Englewood Cliffs, NJ: Prentice-Hall, 1966.
[23] S. A. Schelkunoff and H. T. Friis, *Antennas: Theory and Practice*. New York: Wiley, 1952.
[24] R. F. Harrington and J. R. Mautz, "Straight wires with arbitrary excitation and loading," *IEEE Trans. Antennas Propagat.*, vol. AP-15, pp. 502-515, July 1967.
[25] J. R. Mautz and R. F. Harrington, "Radiation and scattering from bodies of revolution," *Appl. Sci. Res.*, vol. 20, pp. 405-435, June 1969.

Johnson J. H. Wang (M'68-SM'79) was born in Hunan, China, on October 24, 1938. He received the B.S.E.E. degree from National Taiwan University, China, in 1962, the M.S. degree from Florida State University, Tallahassee, in 1965, and the Ph.D. degree from The Ohio State University, Columbus, in 1968.

From 1965 to 1968 he served first as a Research Assistant and later as a Research Associate in The Ohio State University ElectroScience Laboratory. From 1968 to 1975 he worked consecutively at the following industrial firms: Frequency Engineering Laboratory, Farmingdale, NJ; TRW Systems, Redondo Beach, CA; Motorola, Phoenix, AZ; and Texas Instruments, TX. In 1975 he joined the Engineering Experiment Station, Georgia Institute of Technology, Atlanta, as a Senior Research Engineer and is now a Principal Research Engineer. His area of research includes electromagnetic theory, microwaves, antennas, and bioelectromagnetics.

Dr. Wang is a member of the Society of Sigma Xi.

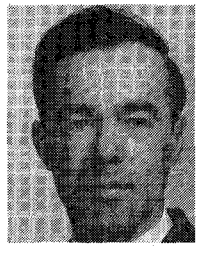

Charles J. Drane (M'65-SM'79) was born in Boston, MA. He received the B.S. degree in physics from Boston College, Newton, MA, in 1950, the S.M. degree in nuclear physics and the S.M. degree in mathematics from the Massachusetts Institute of Technology, Cambridge, MA, in 1954 and 1966, respectively, and the Ph.D. degree in applied physics from Harvard University, Cambridge, MA, in 1975.

In 1952 he was with the Diamond Ordnance Fuze Laboratories of the National Bureau of Standards, Washington, D.C., where he studied conduction properties of germanium diodes. From 1953 until 1955 he was in military service with the U.S. Army, principally at White Sands Proving Ground, NM, where he was engaged in the analysis of missile electronics systems. In 1955 he joined the Antenna Laboratory of the Air Force Cambridge Research Laboratories, Hanscom AFB, MA, which Laboratory in 1976 became the Electromagnetic Sciences Division of the Rome Air Development Center, where he continues to work on various problems in the analysis and synthesis of antenna arrays. Since 1978 he has been a part-time Lecturer in engineering at Northeastern University, Boston, MA, teaching courses in electromagnetic field theory.

Dr. Drane is a member of Sigma Xi and U.S. Commission C, International Scientific Radio Union.